Metals and Materials International (2020) 26:961–972
https://doi.org/10.1007/s12540-019-00370-8

# In-Situ Observation of Martensitic Transformation in a Fe–C–Mn–Si Bainitic Steel During Austempering

**Junyu Tian[1] · Guang Xu[1] · Zhengyi Jiang[2] · Haijiang Hu[1] · Qing Yuan[1] · Xiangliang Wan[1]**

Received: 5 May 2019 / Accepted: 7 July 2019 / Published online: 26 July 2019


**Abstract**
The martensitic transformation in a Fe–C–Mn–Si bainitic steel was examined by in situ high-temperature laser scanning confocal microscopy (LSCM) and dilatometry. The phenomenon of continuous martensitic transformation during austempering was firstly dynamically observed by LSCM. Differing from the commonly accepted viewpoint on martensite formation in bainitic steels, the martensitic transformation in the conventional medium-carbon bainitic steel was not instantaneous and proceeded gradually when the sample was austempered below martensite starting temperature ($M_S$). It can be attributed to the generation of internal stresses, thermal activation, stimulating nucleation, and the segregation of Mn. In addition, apart from the continuous martensitic transformation, the bainitic transformation was also directly observed by LSCM during austempering below $M_S$. Moreover, it was clear from the results of dilatation during austempering that the inflection point in the dilatation curve against time was not the demarcation point between martensitic and bainitic transformation, and in situ observations confirmed that martensite was still formed after the inflection point. Therefore, the obtained results could be an excellent reference to further understand the mechanism of bainitic and martensitic transformations in Fe–C–Mn–Si bainitic steel during austempering below $M_S$.

**Keywords** In-situ · Bainitic steel · Isothermal martensite · Below martensite starting temperature · Segregation

## 1 Introduction

Martensitic transformation plays an important role in improving the mechanical properties of steels [1, 2]. In most advanced high-strength steels (AHSSs), such as dual phase (DP) steels, quenching and partitioning (Q&P) steels, and transformation-induced plasticity (TRIP) steels, their superior mechanical properties are considerably dependent on martensitic transformation [3–8]. Therefore, during the heat treatment of high-strength steels, it is crucial to control the martensitic transformation in order to achieve better mechanical properties.

In recent years, many studies have been conducted on martensitic transformation in steels. Olson and Cohen [9] presented a detailed study on the mechanism of martensitic transformation kinetics in steels. Wang et al. [10] investigated the martensitic transformation behavior of a deformed undercooled austenite and found that it caused a decrease in martensite starting temperature ($M_S$) and formed nanostructured lath martensite with high hardness. However, most of the previous studies on martensite transformation in steels were mainly conducted by traditional optical microscopy (OM), scanning electron microscopy (SEM), and transmission electron microscopy (TEM) techniques.

High-temperature laser scanning confocal microscopy (LSCM) is regarded as an effective approach to study the dynamic phase transformation of martensite and can be used to directly observe the martensitic transformation in steels during the continuous cooling process [11–13]. Ban et al. [11] studied the martensitic transformation in steels by LSCM and advocated that martensite laths were mainly formed on annealed twin boundaries, austenitic boundaries,

✉ Guang Xu
xuguang@wust.edu.cn

[1] The State Key Laboratory of Refractories and Metallurgy, Hubei Collaborative Innovation Center for Advanced Steels, Wuhan University of Science and Technology, Mail Box 131, 947 Heping Avenue, Qingshan District, Wuhan 430081, China

[2] School of Mechanical, Materials, Mechatronic and Biomedical Engineering, University of Wollongong, Wollongong, NSW 2522, Australia

and previously formed laths. Liu et al. [12] directly observed the martensitic transformation in P91 steel by LSCM and claimed that the nucleation of martensite mainly occurred at grain boundaries and grain interiors. Yu et al. [13] adopted LSCM to characterize the microstructural evolution of martensite in a high-strength blast-resistant steel and expressed that the size of martensite packets started to decrease with the increase in prior austenite grain size.

Although the aforesaid studies have investigated the martensitic transformation in steels by in situ LSCM, they mainly focused on the martensitic transformation during the continuous cooling process. The dynamic observations of martensitic transformation in medium-carbon bainitic steels during austempering by LSCM have rarely been carried out. In recent years, the isothermal transformation of bainite austempered below $M_S$ has attracted significant scientific attention [14–16]. Zhao et al. [16] claimed that finer bainite plates with better mechanical properties could be obtained by austempering below $M_S$. It was found that when the austempering temperature was below $M_S$, martensitic transformation, instead of bainitic transformation, occurred first in undercooled austenite. Hence, martensite effectively promoted the subsequent bainitic transformation and led to the refinement of bainite plates. Therefore, the investigation on martensitic transformation occurring before bainitic transformation during an isothermal process is indispensable. The concept of isothermal martensite was first proposed in the early period of the 1990s [17, 18]. Isothermal martensites have been mainly detected by the conventional OM, SEM, or TEM micrographs, thus the direct observation of isothermal martensite transformation by LSCM has been rarely detected. Furthermore, most of the previous studies on isothermal martensite transformation were carried out in alloys with high carbon contents or alloy contents [17, 19, 20]. A very few studies have reported the mechanism of isothermal martensite transformation in traditional bainitic steels; therefore, it is very important to investigate this phenomenon by LSCM. The obtained results might be an excellent reference to further understand the isothermal martensitic transformation as well as the bainitic transformation below $M_S$.

## 2 Materials and Methods

The experimental steel with a chemical composition of Fe-0.36C-1.85Si-2.80Mn (wt%) was first refined in a vacuum induction furnace and cast into a small ingot. The produced ingot was then rolled into a 12-mm thick flat sheet on a four-high rolling mill and air cooled to room temperature. Cylindrical specimens with 7 mm diameter and 4 mm height were machined for LSCM tests. In-situ observations were made on a VL2000DXSVF17SP LSCM system. In order to protect the specimens from surface oxidation, the specimen chamber was initially evacuated to $6\times10^{-3}$ Pa before heating and was filled with argon during the entire heat treatment process. The heating principle of the LSCM experiment can be depicted as follows: the heating chamber was elliptical in shape and its interior was a gold mirror. The light source was at one focus and the tested sample was at another focus. The sample was heated by total reflection and its temperature was adjusted by controlling the light source current. A thermocouple was fixed on the crucible bracket by spot welding and only one temperature is given. In addition, as the area of the uniformly heated soaking space was $\Phi$10 mm × 10 mm and the sample crucible was only 9 mm × 3.5 mm, the whole sample was placed in a homogeneous temperature space during the isothermal process.

The $M_S$ value of the tested steel was found to be 271 °C (calculated by JMatPro 7.0 software), thus the isothermal temperature for martensitic transformation below $M_S$ was selected as 240 °C. The samples were heated to 1000 °C at a rate of 5 °C/s, held for 300 s for austenitization, then cooled to 240 °C at a rate of 5 °C/s, isothermally held for 1800 s for a sufficient transformation, and finally, air cooled to room temperature. LSCM images were continuously recorded at 3 frames/s with 100 × magnification during the entire isothermal treatment. Moreover, a video revealing the transition process from austenite to martensite and bainite was simultaneously obtained. Furthermore, in order to eliminate the effects of segregation, the same LSCM test was conducted after the samples were homogenized at 1300 °C for 5 h. The principle of in situ observation of martensite and bainite nucleation and growth is the relief phenomenon occurring during phase transition [21]. Furthermore, Fig. 1a displays the changes in both thermocouple and programmed temperatures against holding time during the LSCM test. Apart from the temperature undershoot from 240.0 to 235.1 °C, the temperature fluctuation was kept in ± 0.1 °C during the holding process. The small temperature undershoot quickly disappeared in a very short time, it signifies that the effects of temperature fluctuation were inconspicuous.

In order to quantitatively analyze the transformation process, the transformation experiment was carried out on a Gleeble-3500 thermal–mechanical simulator with exactly the same route as that used for LSCM, and cylindrical specimens of 6 mm diameter and 100 mm length were used for this purpose. In order to minimize the effects of temperature gradient during simulations, a couple of copper clamps were used because of its excellent thermal conductivity of copper. It is observable from Fig. 1b that the thermocouple well followed the programmed temperature and the temperature during isothermal holding (in thermal simulation tests) was constant, thus the effects of temperature fluctuation were negligible. The dilatations of the samples were recorded by dilatometry (in the thermal–mechanical simulator) along

the diameter direction. After heat treatment, the final microstructures were observed by a Nova 400 Nano field-emission scanning electron microscope (FE-SEM), a JEM-2100F TEM, and a Zeiss OM. In addition, the energy dispersive spectroscopy (EDS) on FE-SEM was used to analyze Mn segregation.

## 3 Results and Discussion

Figure 2a displays the dilatation curves against temperature during the entire heat treatment process. The slope change at about 500 °C during heating in Fig. 2a may be caused by the dissolution of carbides and the tempering of original phase products. The $Ac_1$ and $Ac_3$ temperatures were measured as 745 °C and 815 °C, respectively. As the austenitization temperature (1000 °C) was higher than $Ac_3$, a full austenite microstructure was obtained at 1000 °C. The point N (310 °C) in Fig. 2a represents the starting point of deviation of the tangent line on the dilatation curve during the cooling process before isothermal heat treatment; it suggests that the transformation occurred at point N. The dilatation versus temperature curve was found to be a straight line during cooling from 1000 °C to 310 °C, indicating that no high-temperature transformation products were formed in this temperature range. Moreover, the inflection point M (~269 °C) signifies an obvious increase in dilatation. Points A and B represent the start and end of the isothermal process, respectively. Points M, A, and B are denoted by points 1, 2, and 3 in Fig. 1b, respectively. Figure 2b exhibits the continuous cooling transformation (CCT) curve (calculated by JMatPro 7.0 software) of the tested steel. The $M_S$ value of the tested steel was 271 °C, and the transformation of ferrites was avoided due to the cooling rate of 5 °C/s. Therefore, it is theoretically confirmed that the phase transition product formed at ~310 °C was bainite.

### 3.1 Transformation During the Cooling Process

The dynamic transformation process was directly observed by high-temperature LSCM. Figure 3a–c displays three frames for a period of 27.36 s. The gradual growth of a sheaf-like unit (marked by arrows) was observed in the temperature range of 329–388 °C. A plot of the length of this unit as a function of time is presented in Fig. 3d, and the slope of the length versus time plot was calculated as 0.67 μm/s. In order to more accurately calculate the growth rate of bainite sheaves, the growth process of other five bainite sheaves growing at different stages was examined, and an average growth rate of 0.58 μm/s was noticed. According to an earlier report [22], the growth rate of bainite in a 0.48C (wt%) steel, calculated by the Zener–Hillert and Bosze–Trivedi models, was in the order of $10^{-3}$ mm/s, which is consistent with the result of the present study. Moreover, the lengthening rate of bainites was far smaller than that of martensite ($10^6$ mm/s) (reported by Xu [23]), confirming that such a slow growing unit is a bainite sheaves. Therefore, it can be inferred that bainite transformation occurred in the temperature range of 329–388 °C. It is worth noting that Fig. 3 only presents an example of the growth rate of one selected bainite sheaf (marked by the white arrow). The growth rate of other bainite sheaves (marked by red arrows) was measured as 0.42 μm/s. It indicates that although the growth rates of different bainite sheaves had a slight difference, they generally followed the results reported in the previous study [22]. The average growth rate of bainite sheaves is considered in the present paper.

The dilatation curve (Fig. 2a) reveals that the bainitic transformation started at 310 °C, whereas it was observed at 388 °C during the in situ observation (Fig. 3a). The main reason for this discrepancy is that LSCM micrographs express the bainitic transformation occurring on the surface of the specimen, whereas dilatation data from the thermal simulator indicate that the bainitic transformation occurred in the interior of the specimen. The surface transformation occurred easily than that in the interior because bainitic reactions are displacive. The displacements occurring in the interior of a specimen cause strains, whereas the strain energy is relieved when the transformation occurs at the free surface. It signifies that bainitic transformation in the proximity of a surface can occur more easily [6]. However, due to a very small amount of bainitic transformation on the surface in the temperature range of 388–310 °C, the transformation was not captured in the dilatation data. Therefore, the bainitic transformation was observed at 388 °C during in situ LSCM, whereas the dilatation data indicate that bainitic transformation occurred at 310 °C. In addition, it may also be attributed to decarburization in the LSCM samples, resulting in the deviation of chemical compositions between the surface and the interior of the specimen. Tomota et al. [24] reported that the decarburization in surface layer of a specimen is observed at high transformation temperature even in vacuum or inert gas atmosphere. It may lead to faster and easier transformation in the surface than in the interior. The dynamic transformation process of other units was directly observed by high-temperature LSCM. Figure 4 reveals the formation of martensite during cooling from $M_S$ (269 °C) to the thermal holding temperature of 240 °C. When the specimen was cooled to ~259 °C (below $M_S$), the dark units marked by ellipses appeared (Fig. 4b); however, they were not present in Fig. 4a, and the time difference between these two frames of the video was 0.33 s. Other units marked by ellipses (Fig. 4d), also appeared suddenly (not observed in Fig. 4c). The growth of these units was so fast that the growth process could not be captured. The real growth velocities of these units should be higher

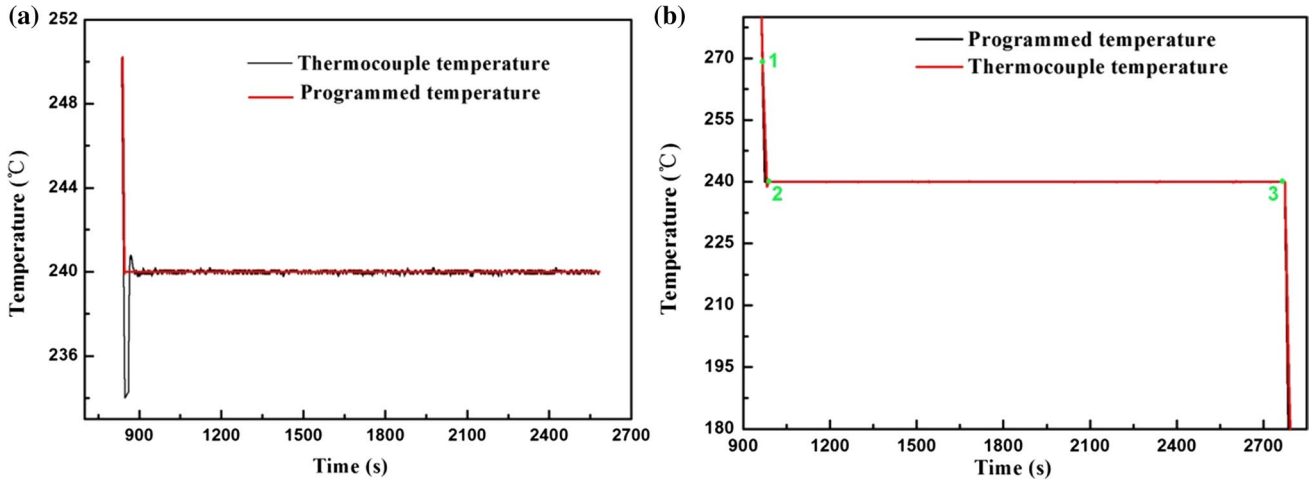


**Fig. 1** The curves of thermocouple and programmed temperature versus holding time: **a** during LSCM test; and **b** during the thermal simulation test

than the value obtained by dividing lengths by the frame interval of 0.33 s, thus the real velocities of these fast-growing units could not be obtained by the current observation. The growth rate of bainites in 0.48C (wt%) steel was of the order of $10^{-3}$ mm/s (calculated by the Zener–Hillert and the Bosze–Trivedi models) [12, 25]. In the present study, the growth rate of these black units was significantly higher than that of a bainite sheaf. Moreover, the transformation temperature was 259.1 °C, which was below the $M_S$ of the experimental steel. Therefore, it can be inferred that the rapidly growing units marked by ellipses were martensite plates.

In order to clearly measure the growth rate of martensite laths in LSCM, the time interval between the two frames during the cooling process from 300 to 240 °C was shortened by ten folds (the frame interval of 0.33 s was reduced to 0.033 s). The growth of black units in the homogenized sample is displayed in Fig. 5. It is noticeable that the growth of black units was so fast that it still could not be captured. Therefore, martensite and bainite were mainly distinguished by their transformation rates. Additionally, martensite and bainite could also be determined based on their micromorphologies [martensite are thick and black plates (instantaneous growth), whereas bainite are thin and light grey plates (slow growth)].

It should be also noted that the black unit appeared at 278.3 °C in homogenized sample, which is higher than in sample without homogenization. It can be attributed to the increase in $M_S$ due to larger prior austenite grain size (PAGS) caused by the high-temperature annealing process. According to the LSCM micrograph after austenization, the average grain sizes of samples with homogenization and without homogenization are calculated by the software of

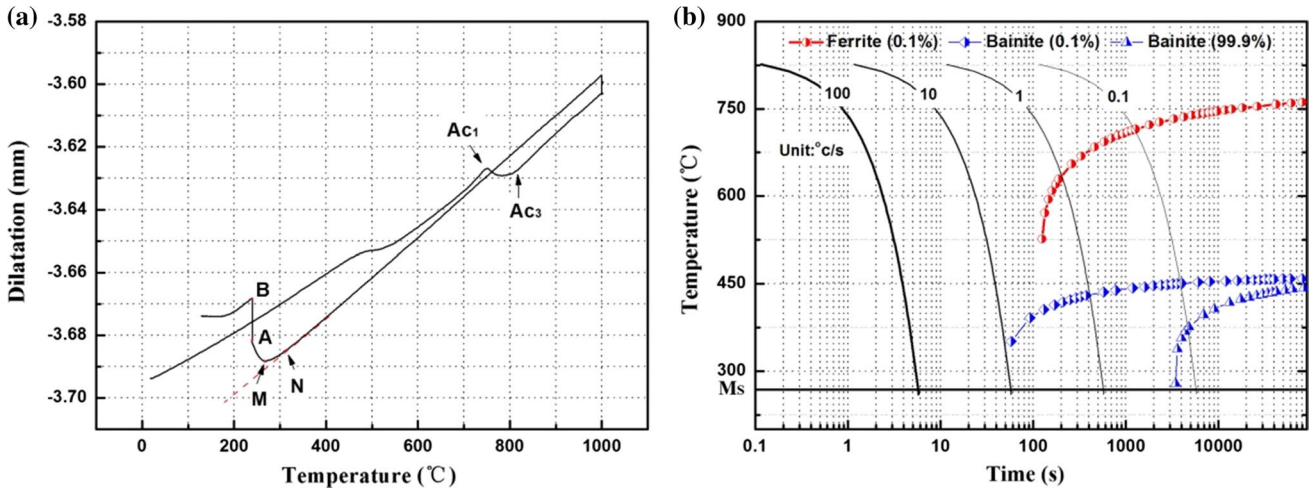


**Fig. 2** **a** The dilatation versus temperature during the entire heat treatment and **b** the CCT curves of the tested steel

Image-Pro Plus based on the diagonal method. The average grain sizes of different samples with homogenization and without homogenization were 105.7 ± 9.3 μm and 60.4 ± 7.6 μm, respectively. It shows that the average grain size increases obviously after high-temperature annealing process. It is consistent with the result reported by Hanamura et al. [26] that the value of $M_S$ increased with an increase in PAGS.

### 3.2 Transformation During Austempering

Figure 6 shows the growth of two growing units (marked as B1 and B2) during austempering. The time interval between Fig. 6a, b is 22.31 s. Based on the lengths of the growing units at different times, the slope of the lengthening curve was calculated as 0.72 μm/s, and this result is very close to the growth rate of bainite (0.58 μm/s) observed during continuous cooling; therefore, B1 and B2 could be assumed as bainite sheaves. It confirms that bainite could be formed at temperatures below $M_S$.

Figure 7 presents a series of frames that reveals the rapid growth of some black units during austempering at 240 °C, and these rapidly growing units (marked by arrows) were not present in the previous frame of the video. As mentioned in Sect. 3.1, in the time interval of 0.033 s between two frames, these black units grew so fast that it was not possible to catch their growth process; therefore, these rapidly growing units can be assumed to be martensite plates. Based on the evolving microstructures in Figs. 6 and 7, it can be deduced that both martensite and bainite were formed during austempering below $M_S$. In addition, it should be noted that although the martensitic transformation from macroscopical phenomenon continuously occurred at a slow speed over time, the growth rate of each martensite lath was extremely high and the growth process could not be captured by the current observation even the time interval was 0.033 s.

Moreover, these black growing units (martensite laths) shown in Fig. 7a–f appeared over a time interval of ~ 420 s from 837.39 to 1257.37 s during austempering. This phenomenon differs from the previously held viewpoint where martensitic transformation is expected to be finished in a very short period of time after a sample is cooled to a certain temperature below $M_S$ because of the diffusionless nature of martensite transformation in conventional medium-carbon bainitic steels. The following reasons could be attributed to the formation of martensite laths in several bursts over an extended period of time. First, the formation of martensite and bainite before the holding process generated internal stresses inside untransformed austenite, in turn, large stresses in austenite stopped the further formation of martensite. However, with an increase in holding time, stresses, especially, at the surface of the specimen, became relaxed

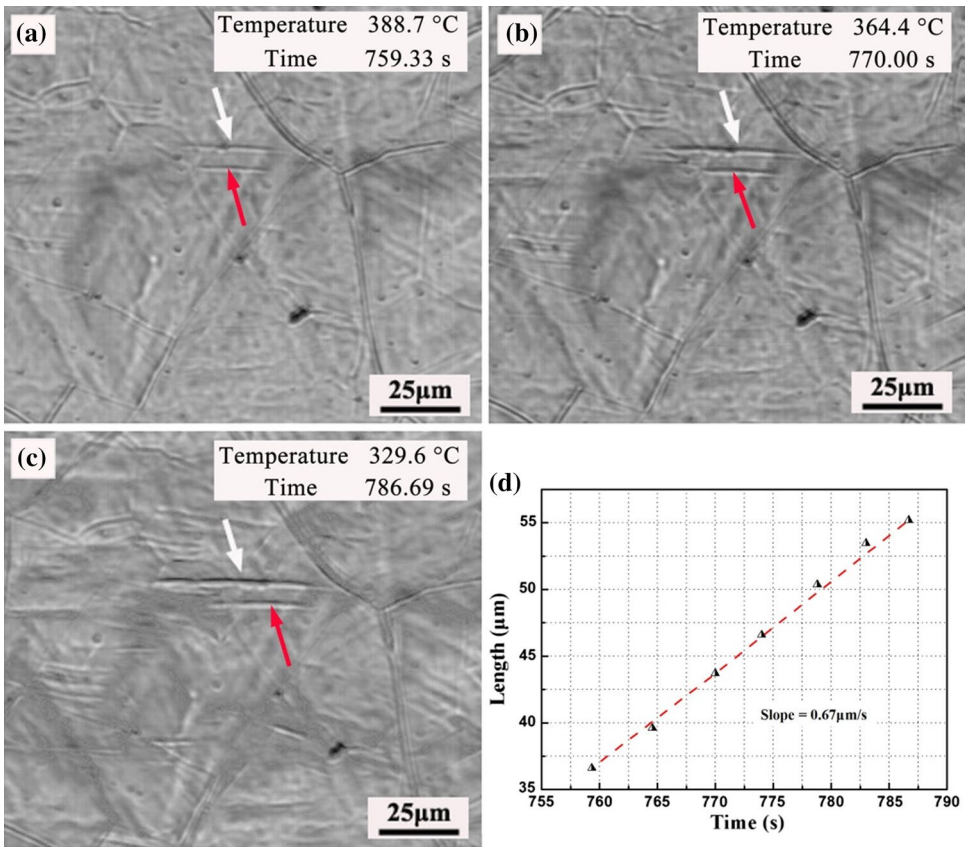


**Fig. 3** The gradual growth of a slow-growing unit during the cooling process above MS: (**a**) 388.7 °C, 759.33 s; (**b**) 364.4 °C, 770.00 s; (**c**) 329.6 °C, 786.69 s and (**d**) the length-to-time plot showing the lengthening rate

gradually due to recovery, thus more martensites were formed. Second, thermally activated, i.e. some martensite embryos that would have required a lower temperature for thermal nucleation needed more isothermal time for nucleation. Third, the time-dependent nucleation was stimulated by the continuous growth of martensite units. Finally, as the experimental steel contained 2.80 wt% Mn, it led to the Mn segregation problem. Figure 8a, b, respectively, display OM and SEM microstructures of the specimen without homogenization after heat treatment. It is evident that the problem of Mn segregation existed even after austenitization, thereby resulting in the appearance of martensite at different stages of heat treatment due to the presence of Mn-depleted and Mn-rich regions. The martensite transformation occurred more easily in Mn-depleted regions before the holding process, and consequently, it generated more carbon atoms and larger strains in surrounding untransformed austenite and retarded the subsequent isothermal martensite transformation. Therefore, the segregation of Mn affected the observed phenomenon at a large extent.

### 3.3 Effects of Segregation on Martensitic Transformation

In order to explore the effects of rich and poor Mn contents on $M_S$ and bainitic transformation kinetics, the CCT curves of different samples with two assumed Mn contents (2.0 wt% Mn in Mn-depleted regions and 3.5 wt% Mn in Mn-rich regions) were calculated by JMatPro 7.0 software, and the corresponding results are illustrated in Fig. 9. It shows that the increase of Mn moves the CCT curves right and down, indicating that the increase of Mn content retards the transformation. In addition, it is noticeable that the increase of Mn contents from 2.0 to 3.5 wt% results in the decrease of $M_S$ from 293.1 to 230.0 °C. The increase of $M_S$ would lead to the increase of the amount of athermal martensite (AM) before holding process, resulting in the less amount of untransformed austenite for the subsequent isothermal martensite transformation. In order to quantitatively analyze the effect of Mn segregation on the volume fraction of AM, Eqs. (1) and (2) are used to calculate the $V_{AM}$ in rich-Mn and poor-Mn regions [27]. The calculations were performed for the upper and lower ranges of concentrations of Mn (2.0–3.5 wt%), whereas the concentrations of the remaining elements were considered as the nominal composition.

$$K_{BS} = 0.0224 - 0.0107x_C - 0.0007x_{Mn} - 0.00005x_{Ni} - 0.00012x_{Cr} - 0.0001x_{Mo} \quad (1)$$

$$V_{AM} = 1 - \exp\left[-K_{BS} \cdot \left(M_S - T\right)\right] \quad (2)$$

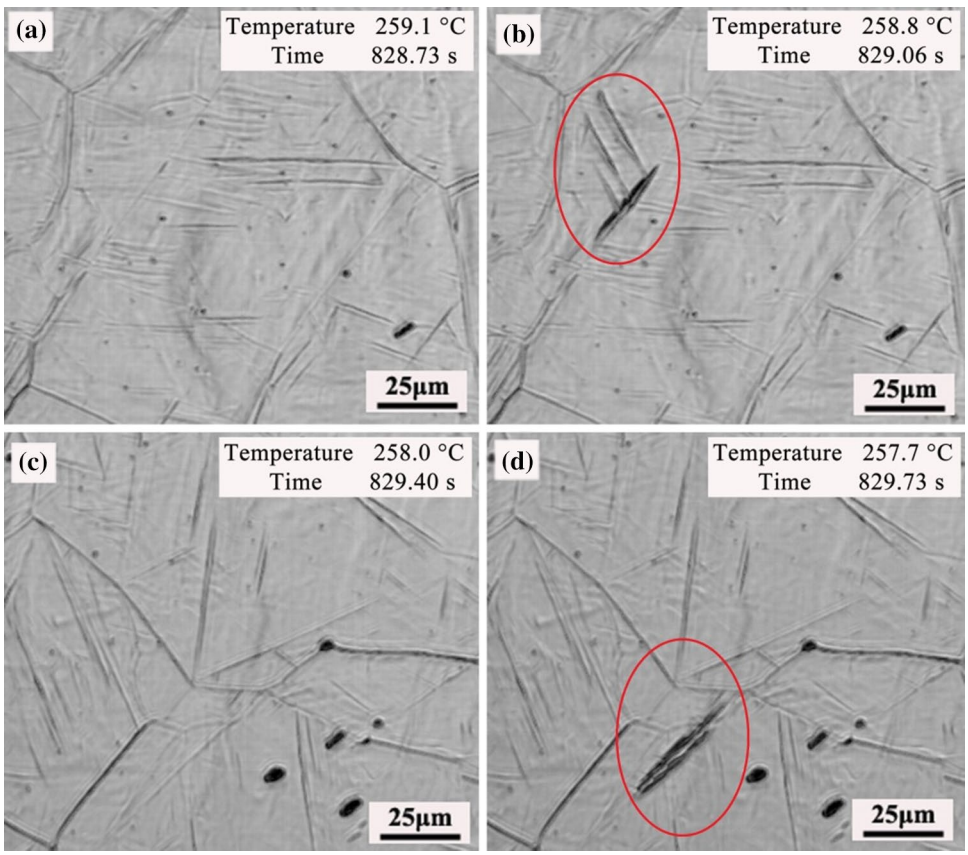


**Fig. 4** The growth of martensite laths during the cooling process above MS: (**a**) 259.1 °C, 828.73 s; (**b**) 258.8 °C, 829.06 s; (**c**) 258.0 °C, 829.40 s and (**d**) 257.7 °C, 829.73 s

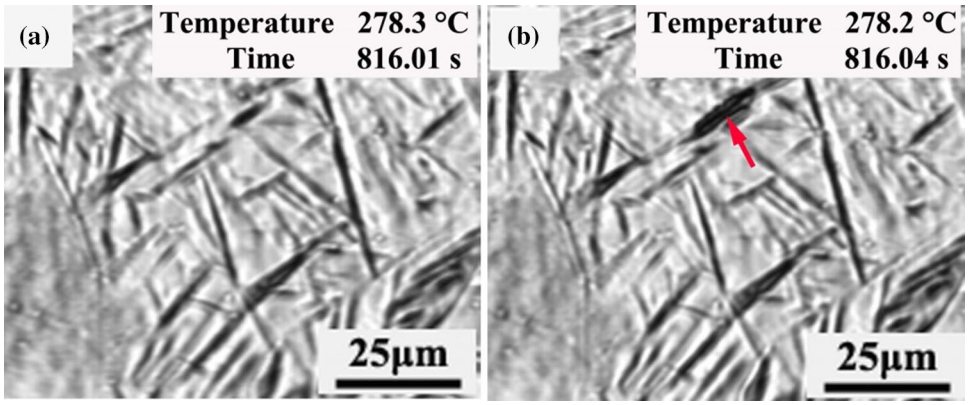


**Fig. 5** An example of the growth of martensite laths between two frames with a time interval of 0.033 s, indicating the fast growth of martensite laths: (**a**) 278.3 °C, 816.01 s; (**b**) 278.2°C, 816.04 s

where $x_i$ represents the mass percent of element "$i$", T is the austempering temperature (240 °C in the present study). Based on Eq. (1), the values of $K_{BS}$ for rich-Mn and poor-Mn regions were calculated to be 0.017148 and 0.016098 $°C^{-1}$, respectively. Then, according to the values of $K_{BS}$ and $M_S$ of different regions, the volume fractions of AM were calculated by Eq. (2), and the results are 59.7% for poor-Mn region and 0.0% for rich-Mn region (because the $M_S$ is below the isothermal temperature), respectively. It indicates that the segregation of Mn has a great influence on martensitic transformations.

In order to further clarify the effects of Mn segregation on the observed phenomenon, the tested steel was homogenized at 1300 °C for 5 h. The same heat treatment process was carried out once again in the homogenized sample by LSCM. Figure 10a, b, respectively, exhibit OM and SEM microstructures of the homogenization sample after LSCM, whereas Fig. 10c reveals the original microstructure of the homogenized sample before LSCM. Figure 10d presents the microstructure of the homogenized sample after direct quenching without holding in LSCM. It is noticeable that the effects of Mn segregation were significantly reduced after high-temperature annealing. In addition, to check the Mn segregation in homogenization sample, face scanning and line scanning tests of the sample were conducted and the corresponding results are given in Fig. 10e. It shows that there is no obvious difference in Mn content in the whole observed region. Therefore, the effect of Mn segregation on the isothermal martensite transformation is very small for the homogenized sample.

Figure 11 presents a series of frames that illustrates the growth of some martensite laths in the homogenized sample during austempering at 240 °C. Although the time interval of isothermal martensite transformation was shortened to ~ 220 s, the successive process of isothermal martensite still occurred in the homogenized sample, hence, it indicates that Mn segregation had a great influence on the successive process of isothermal martensites (however, it is not a unique factor). Hajyakbary et al. [28] reported that long high-temperature homogenization treatments are rarely used in the elimination of Mn segregation in industrial sectors because it is beyond the range of economic feasibility. Therefore, it is crucial to investigate the effects of Mn segregation on martensitic transformation.

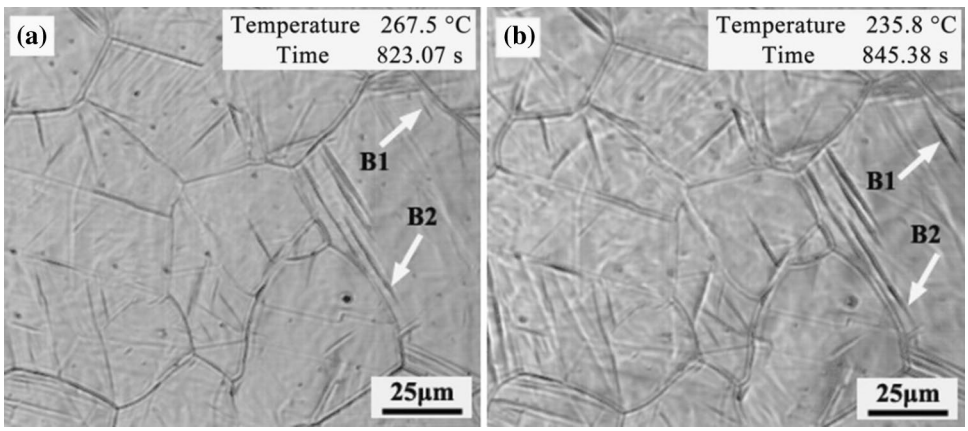


**Fig. 6** The growth of slow-growing unit during the austempering process: (**a**) 267.5 °C, 823.07 s; (**b**) 235.8 °C, 845.38 s

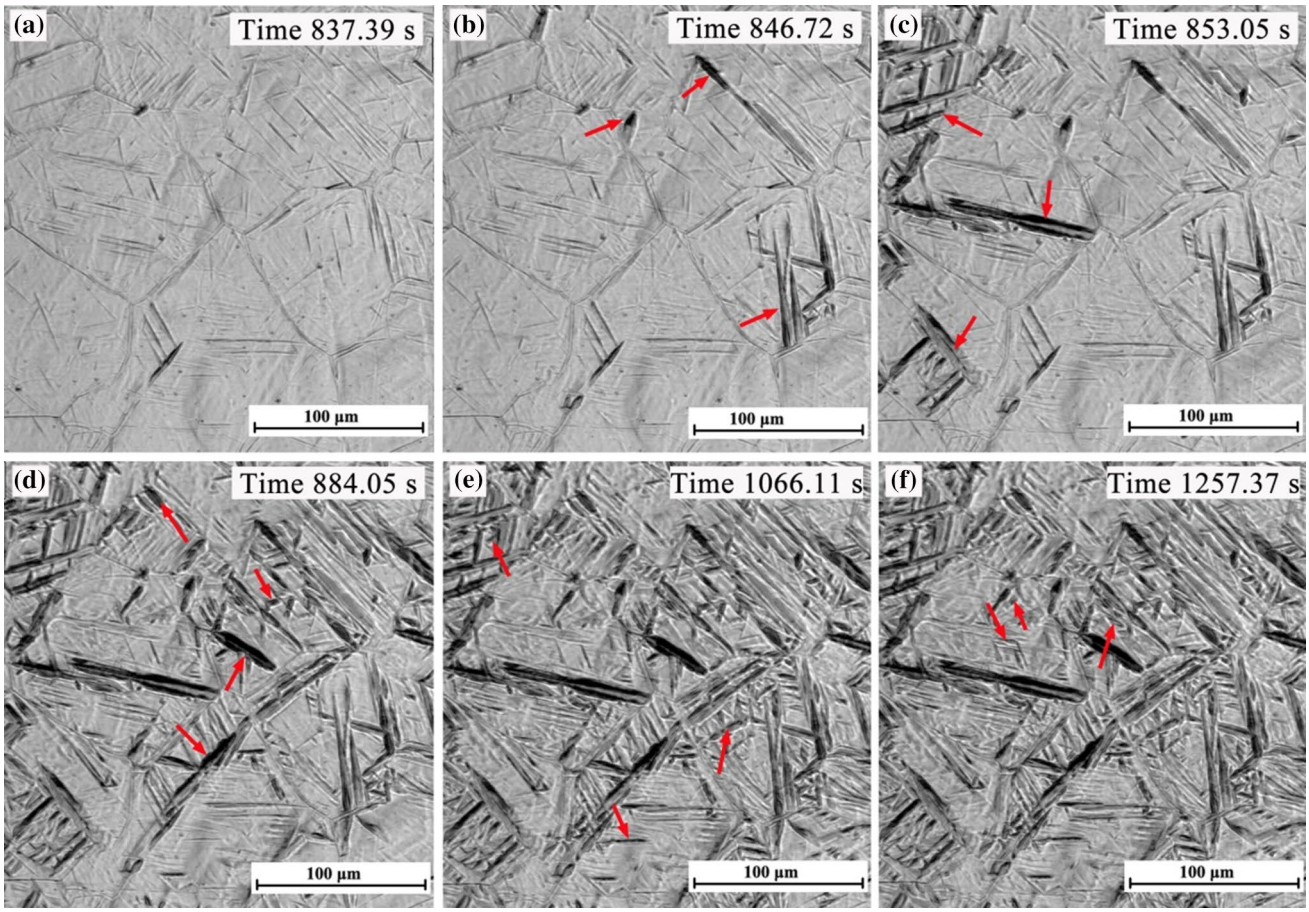


**Fig. 7** The growth of martensite laths during the austempering process at 240 °C: (**a**) 837.39 s; (**b**) 846.72 s; (**c**) 853.05 s; (**d**) 884.05 s; (**e**) 1066.11 s and (**f**) 1257.37 s

### 3.4 Dilatation Data

The dilatation curve against time during austempering of sample without homogenization is plotted in Fig. 12a, and the dilatation curve against time during the whole cooling and austempering processes is presented in Fig. 12b. It should be noted that points M′, A′, and B′ in Fig. 12a, respectively, correspond to points M, A, and B in Fig. 2a because they came from the same group of thermal simulation experimental data. Point M′ represents the starting

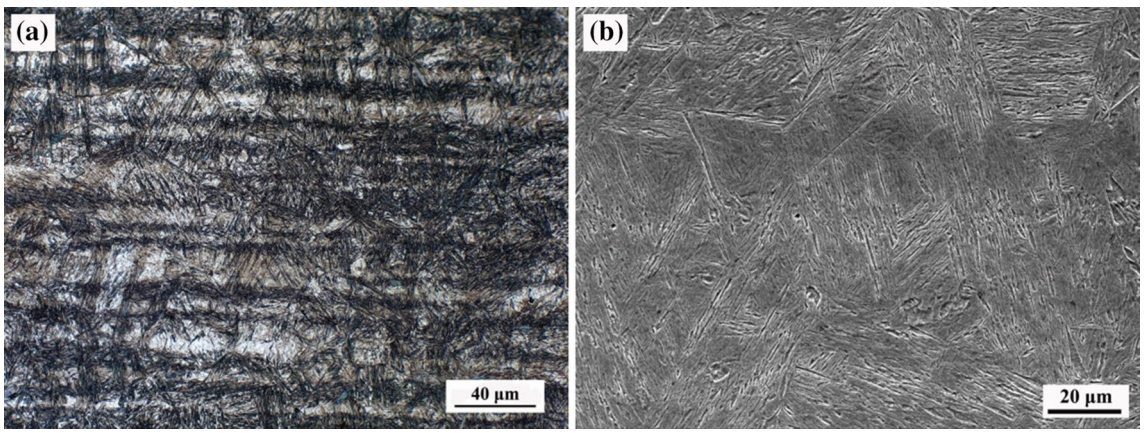


**Fig. 8** The microstructure of steel showing segregation after heat treatment: **a** OM and **b** SEM

point of martensitic transformation and point A′ indicates the beginning of the holding process. It is observable from Fig. 12a that dilatation increased dramatically before the beginning of isothermal transformation in M′A′ segment and the beginning period of the isothermal transformation (A′A″). However, after point A″, the increasing trend in dilatation tended to slow down significantly. The rapid increase in dilatation could be caused by the formation of athermal martensite (AM), whereas the isothermal bainitic transformation may be the reason for the slow increase in dilatation [16, 29, 30]. It is well known that bainite transformation in medium or high-carbon bainitic steels is generally accompanied by a certain incubation period and follows the "S" curve [6]. However, in the present study, no clear incubation period instead of the increase in dilatation at the beginning of transformation (A′A″) was noticed. It indicates that bainite transformation was greatly promoted by AM transformation (M′A′) before the holding process. Furthermore, according to the previous results, point A′ (beginning point of the holding process) in the dilatation curve can be regarded as the demarcation point between martensitic and bainitic transformations because of the diffusionless transformation of martensite. However, it is discernible from the LSCM results that martensitic transformation mainly occurred in the first 420 s in the unhomogenized sample and in the first 220 s in the homogenized sample during the isothermal process. It implies that the beginning point of the holding process in the dilatation curve was not the demarcation point between martensitic and bainitic transformations in the present study. Therefore, dilation after the demarcation point A′ could not represent the amount of bainite transformation, this finding is different from the results reported by earlier researchers [16, 29], and this is another main novelty of the present work.

In addition, it is clear in Figs. 12a and 7f that the amount of transformed martensite in LSCM was larger than that in the thermal simulator. It happened because LSCM micrographs reveal the bainitic transformation on the surface of the specimen, whereas dilatation data of the thermal simulator represents the bainitic transformation in the interior of the specimen. The surface transformation occurred easier than that in the interior because strain energies were relieved more easily when the transformation occurred at the free surface [6].

Figure 13 presents the TEM microstructure of the sample after ausforming. Martensite and bainite were both present in the microstructure, and some carbides were also observed in martensite laths. Carbides were precipitated from AM in the subsequent isothermal process [30]. The continuous precipitation of carbides during the holding process is conductive to the subsequent AM and bainite transformation because the carbides precipitation provides more nucleation sites for subsequent transformation. It may also result in the incessant formation of isothermal martensite. In addition, TEM results indicate that AM was formed before isothermal bainite.

Previous studies [16, 29] on the isothermal transformation of bainitic steels below $M_S$ suggested that martensitic transformation was completed instantaneously, and it is inconsistent with the LSCM results in the present paper. In addition, although the mechanism of isothermal martensitic transformation has been reported previously [17, 18], most researchers mainly observed this phenomenon in high-carbon or high-alloy steels by pure metallographic methods, and reasonable explanations for isothermal martensite transformation were not presented [17, 19, 20, 31]. In the present paper, the phenomenon of continuous martensitic transformation in conventional medium-carbon bainitic steel during austempering was firstly dynamically observed by

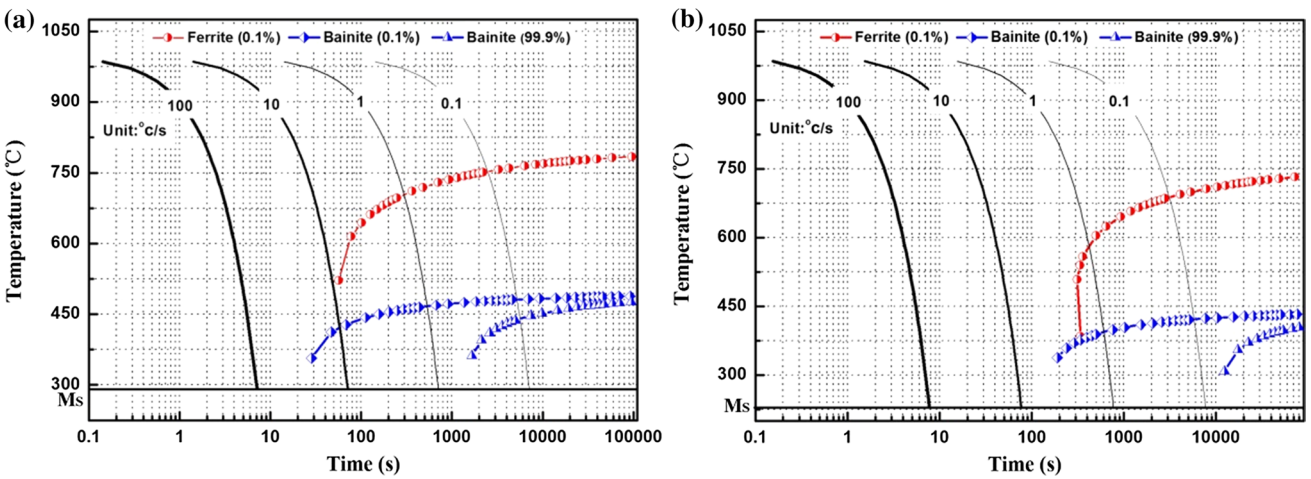


**Fig. 9** The CCT curves of the tested steel with different samples: **a** with 2.0 wt% Mn; and **b** with 3.5 wt% Mn

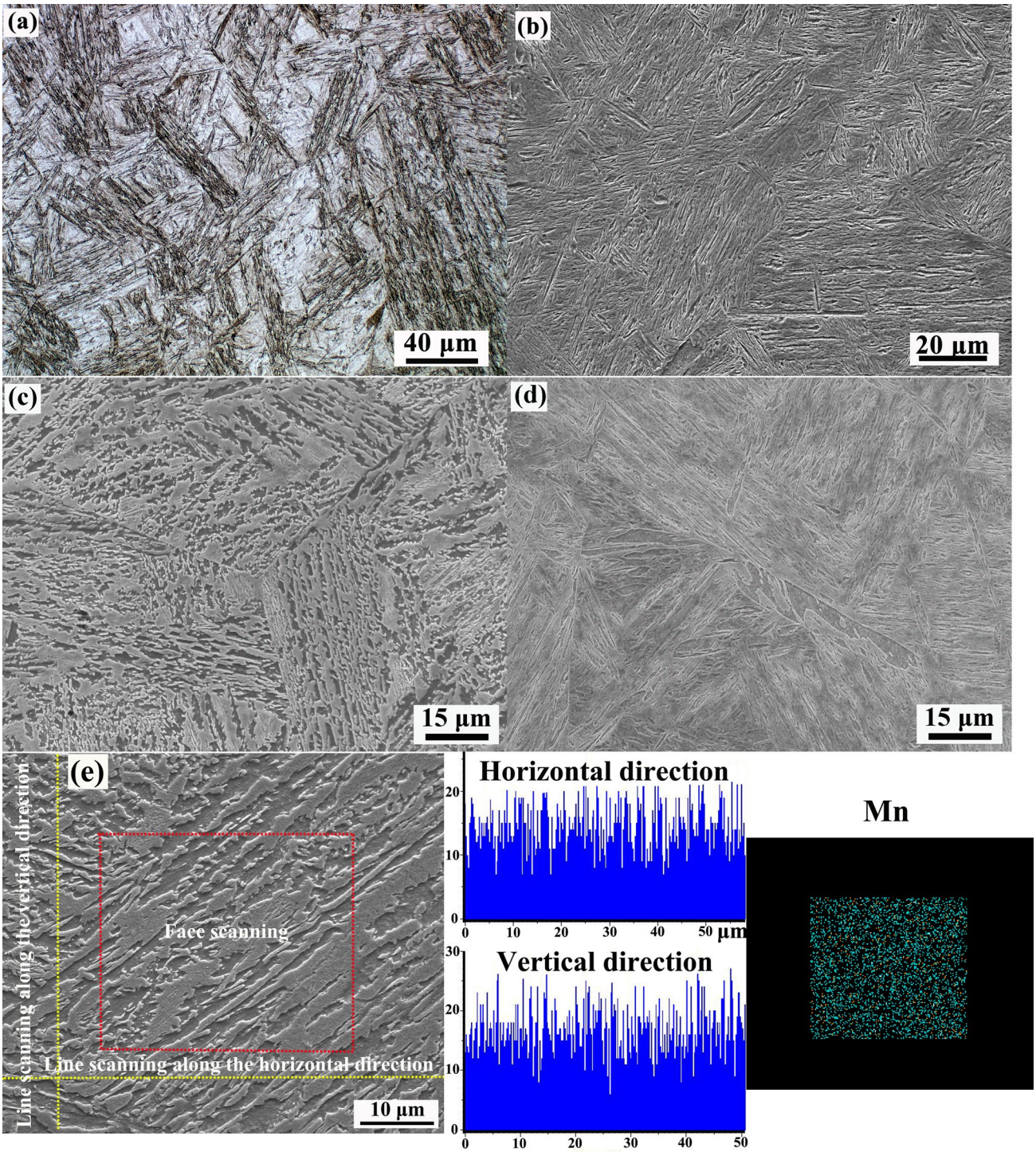


**Fig. 10** The microstructures of homogenization sample: **a** OM and **b** SEM after the whole LSCM experiment; **c** the original SEM microstructure before LSCM; **d** the SEM microstructure after direct quenching; and **e** the face and line scanning results of Mn

LSCM, and the corresponding explanations were presented. The obtained results could be useful to further understand bainitic and martensitic transformations at temperature below $M_S$ and provide a theoretical reference to achieve an optimized heat treatment technology for medium-carbon bainitic steels.

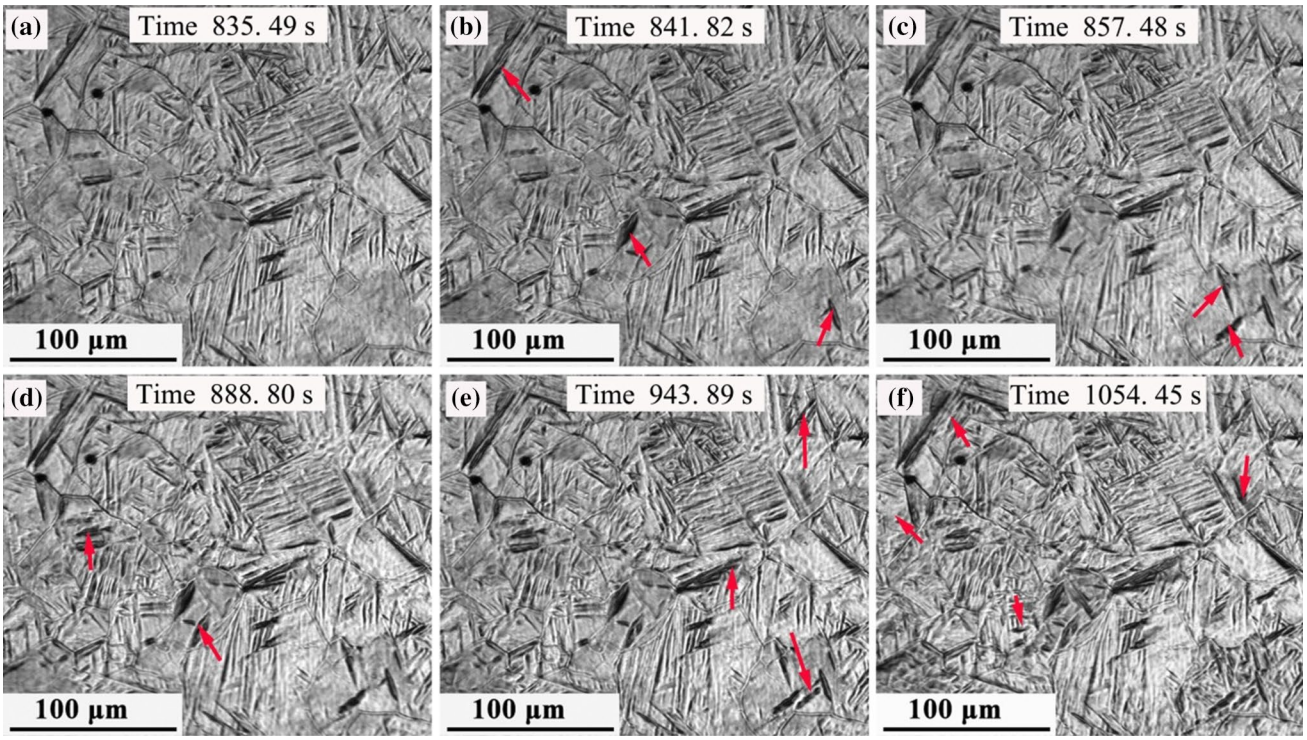


**Fig. 11** The growth process of martensite laths in high-temperature annealing sampleduring the austempering process at 240 °C: (**a**) 835.49 s; (**b**) 841.82 s; (**c**) 857.48 s; (**d**)888.80 s; (**e**) 943.89 s and (**f**) 1054.45 s

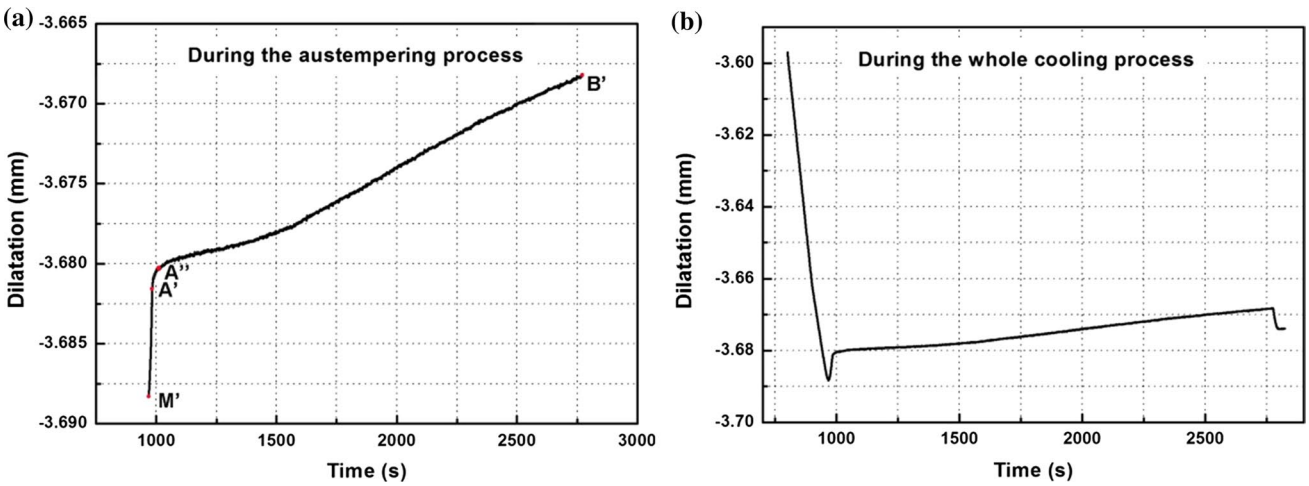


**Fig. 12** The curve of dilatation versus time **a** during the austempering process and **b** during the whole cooling and holding process

## 4 Conclusions

In the present study, the continuous martensitic transformation in a Fe–C–Mn–Si bainitic steel during austempering below $M_S$ was firstly observed by in situ LSCM. Differing from the previously accepted viewpoint, the martensitic transformation in the medium-carbon bainitic steel did not finish instantaneously but occurred in a drawn-out fashion as time progressed during the austempering process. It took ~ 420 s for the unhomogenized sample and ~ 220 s for the homogenized sample to complete martensitic transformation during the isothermal transformation at temperature below $M_S$. Moreover, during austempering, the inflection point in the dilatation curve against time was not the demarcation point between martensitic and bainite transformations. After the inflection point, the martensite phase

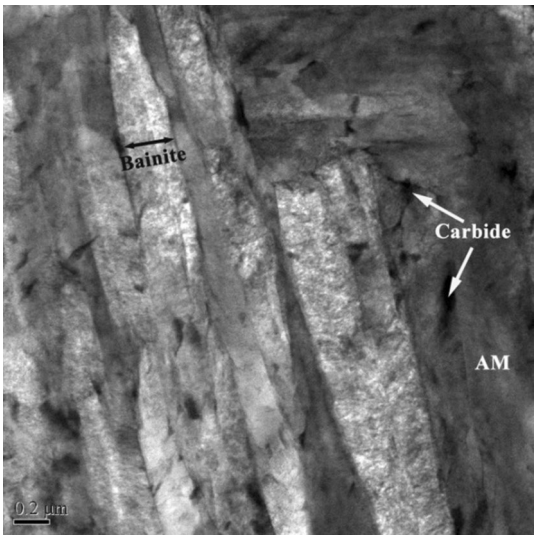


**Fig. 13** TEM microstructure of the sample

transition still persisted with time; therefore, the dilatation occurring after the inflection point could not be used to determine the amount of bainitic transformation.

**Acknowledgements** This work is supported by National Natural Science Foundation of China [Nos. 51874216 & 51704217]; Major Projects of Technological Innovation in Hubei [No.2017AAA116]; Hebei Joint Research Fund for Iron and Steel [E2018318013]; and the State Scholarship Fund of China Scholarship Council.

## References

1. A. Bag, K.K. Ray, E.S. Dwarakadasa, Metall. Mater. Trans. A **30**, 1193 (1999)
2. A. Kumar, S.B. Singh, K.K. Ray, Mater. Sci. Eng. A **474**, 270 (2008)
3. J.W. Zhao, Z.Y. Jiang, Prog. Mater Sci. **94**, 174 (2018)
4. J.Y. Tian, G. Xu, Z.Y. Jiang, H.J. Hu, M.X. Zhou, Met. Mater. Int. **24**, 1202 (2018)
5. D.M. Xu, G.Q. Li, X.L. Wan, R.L. Xiong, G. Xu, K.M. Wu, M.C. Somani, R.D.K. Misra, Mater. Sci. Eng. A **688**, 407 (2017)
6. G. Xu, F. Liu, L. Wang, H.J. Hu, Scr. Mater. **68**, 833 (2013)
7. H.J. Hu, G. Xu, L. Wang, Z.L. Xue, Y.L. Zhang, G.H. Liu, Mater. Des. **84**, 95 (2015)
8. Y. Tomita, K. Morioka, Mater. Charact. **38**, 243 (1997)
9. G.B. Olson, M. Cohen, Metall. Trans. A **7**, 1915 (1976)
10. T.S. Wang, M. Zhang, Y.H. Wang, J. Yang, F.C. Zhang, Scr. Mater. **68**, 162 (2013)
11. L.L. Ban, J. Wen, X.X. Shi, W.P. Liu, Metall. Anal. **31**, 1 (2011)
12. Z.C. Liu, Y.P. Ji, Z.P. Hei, H.P. Ren, Trans. Mater. Heat. Treat. **35**, 96 (2014)
13. X. Yu, S.S. Babu, J.C. Lippold, H. Terasaki, Y.I. Komizo, Metall. Mater. Trans. A **43**, 1538 (2012)
14. I.A. Yakubtsov, G.R. Purdy, Metall. Mater. Trans. A **43**, 437 (2012)
15. S. Samanta, P. Biswas, S. Giri, S.B. Singh, S. Kundu, Acta Mater. **105**, 390 (2016)
16. L. Zhao, L. Qian, J. Meng, Q. Zhou, F.C. Zhang, Scr. Mater. **112**, 96 (2016)
17. H. Okamoto, M. Oka, Metall. Trans. A **16**, 2257 (1985)
18. A. Borgenstam, M. Hillert, Acta Mater. **45**, 651 (1997)
19. G. Ghosh, Philos. Mag. A **71**, 333 (2016)
20. H. Pal, A. Chanda, M. De, J. Alloys Compd. **278**, 209 (1998)
21. T. Ko, S.A. Cottrell, J. Iron Steel Inst. **172**, 307 (1952)
22. Y.Z. Zhu, J.P. Xu, Int. J. Min. Met. Mater. **19**, 821 (2012)
23. Z.Y. Xu, *Martensite Transformation and Martensite* (Science Press, Beijing, 1980). **(In Chinese)**
24. Y. Tomota, Y.X. Wang, T. Ohmura, N. Sekido, S. Harjo, T. Kawasaki, W. Gong, A. Taniyama, ISIJ Int. **58**, 2125 (2018)
25. Z.W. Hu, G. Xu, H.J. Hu, L. Wang, Z.L. Xue, Int. J. Min. Met. Mater. **21**, 371 (2013)
26. T. Hanamura, S. Torizuka, S. Tamura, S. Enokida, H. Takech, Mater. Sci. Forum **783–786**, 1027 (2014)
27. S.J. Lee, C.J.V. Tyne, Metal. Mater. Trans. A **43**, 422 (2012)
28. F. Hajyakbary, J. Sietsma, R.H. Petrov, G. Miyamoto, T. Furuhara, M.J. Santofimia, Scr. Mater. **137**, 27 (2017)
29. E.P.D. Silva, D.D. Knijf, W. Xu, C. Föjer, Y. Houbaert, J. Sietsma, Mater. Sci. Technol. **31**, 808 (2015)
30. J.Y. Tian, G. Xu, M.X. Zhou, H.J. Hu, Steel Res. Int. (2018). https://doi.org/10.1002/srin.201700469
31. M. Oka, H. Okamoto, Metall. Trans. A **19**, 447 (1988)